Sideways: Depth-Parallel Training of Video Models

Mateusz Malinowski[1], **Grzegorz Świrszcz**[1], **João Carreira**[1] **and Viorica Pătrăucean**[1]
[1]DeepMind

We propose *Sideways*, an approximate backpropagation scheme for training video models. In standard backpropagation, the gradients and activations at every computation step through the model are temporally synchronized. The forward activations need to be stored until the backward pass is executed, preventing inter-layer (depth) parallelization. However, can we leverage smooth, redundant input streams such as videos to develop a more efficient training scheme? Here, we explore an alternative to backpropagation; we overwrite network activations whenever new ones, i.e., from new frames, become available. Such a more gradual accumulation of information from both passes breaks the precise correspondence between gradients and activations, leading to theoretically more noisy weight updates. Counter-intuitively, we show that *Sideways* training of deep convolutional video networks not only still converges, but can also potentially exhibit better generalization compared to standard synchronized backpropagation.

Keywords: Computer Vision, Deep Learning, BackPropagation, Parallel Training

arXiv:2001.06232v1 [cs.LG] 17 Jan 2020



Figure 1 | Three frames of a fish swimming, sampled 15 frames apart, or about every half a second. Note how little variation there is in the patch within the red square. Can we leverage such redundancies and the smoothness in local neighborhoods of such type of data for more efficient training? Our results suggest we can and there could be generalization benefits in doing that.

1. Introduction

The key ingredient of deep learning is stochastic gradient descent (SGD) [6, 41, 53], which has many variants, including SGD with Momentum [47], Adam [24], and Adagrad [12]. SGD approximates gradients using mini-batches sampled from full datasets, and thus it differs from standard gradient descent. Efficiency considerations primarily motivated the development of SGD as many datasets do not fit in memory. Moreover, computing full gradients over them would take a long time, compared to mini-batches, i.e., performing SGD steps is often more preferred [6, 14, 53]. However, SGD is not only more efficient but also produces better models. For instance, giant-sized models trained using SGD are naturally regularized and may generalize better [16, 42], and local minima do not seem to be a problem [9]. Explaining these phenomena is still an open theoretical problem, but it is clear that SGD is doing more than merely optimizing a given loss function [52].

In this paper, we propose a further departure from the gradient descent, also motivated by efficiency considerations, which trains models that operate on sequences of video frames. Gradients of neural networks are computed using the backpropagation (BP) algorithm. However, BP operates in a *synchronized* blocking fashion: first, activations for a mini-batch are computed and stored during the forward pass, and next, these activations are re-used to compute Jacobian matrices in the backward pass. Such blocking means that the two passes must be done sequentially, which leads to high latency, low throughput. This is particularly sub-optimal if there are parallel processing resources available, and is particularly prominent if we cannot parallelize across batch or temporal dimensions, e.g., in online learning or with causal models.

The central hypothesis studied in this paper is whether we can backpropagate gradients based on activations from different timesteps, hence removing the locking between the layers. Intuitively, one reason this may work is that high frame rate videos are temporally smooth, leading to similar representations of neighboring frames, which is illustrated in Figure 1.

Corresponding author: mateuszm@google.com
© 2023 DeepMind. All rights reserved

We experiment with two types of tasks that have different requirements in terms of latency: a per-sequence action recognition, and a per-frame autoencoding. In both cases, our models do not use any per-frame blocking during the forward or backward passes. We call the resulting gradient update procedure *Sideways*, owing to the shape of the data flow, shown in Figure 2.

In experiments on action recognition, UCF101 [45] and HMDB51 [27], we have found that training with *Sideways* not only does not diverge but often has led to improved performance over *BP* models, providing a surprising regularization effect. Such training dynamics create a new line of inquiry into the true nature of the success of SGD, as it shows that it is also not critical to have precise alignment between activations and gradients. Additionally, we show that *Sideways* provides a nearly linear speedup in training with depth parallelism on multiple GPUs compared to a *BP* model using the same resources. We believe that this result also opens up possibilities for training models at higher frame rates in online settings, e.g., where parallelization across mini-batches is not an option.

We use per-frame autoencoding task to investigate the effect of the blocking mechanism of *BP* models in tasks where the input stream cannot be buffered or where we require immediate responses. This is particularly problematic for *BP* if the input stream is quickly evolving, i.e., the input change rate is higher than the time required to process the per-step input. In this case, the blocking mechanism of *BP* will result in discarding the new inputs received while the model is being blocked processing the previous input. However, this is considerably less problematic in *Sideways* due to its lock-free mechanism. We run experiments on synthetically generated videos from the CATER dataset [13], where we observe that *Sideways* outperforms the *BP* baseline.

2. Related Work

Our work connects with different strands of research around backpropagation, parallelization and video modelling. We list here a few of the most relevant examples.

Alternatives to backpropagation. Prior work has shown that various modifications of the 'mathematically correct' backpropagation can actually lead to satisfactory training. For instance, some 'relaxations' of backpropagation implemented with a fixed random matrix yield a surprisingly good performance on MNIST [29]. There is also a recent growing interest in building more biologically-plausible approaches such as Feedback Alignment [29], Direct Feedback Alignment [36], Target Propagation [4], Kickback [2], and Synthetic Gradients [21], where various decouplings between forward and backward passes are proposed. A good comparative overview of those frameworks is presented at [10]. Another recent innovative idea is to meta-learn local rules for gradient updates [33], or to use either self-supervised techniques [38] or local losses to perform gradient-isolated updates locally [31, 37]. Asynchronous distributed SGD approaches like Hogwild [40] also do not strictly fit into clean backprop as they allow multiple workers to partially overwrite each others weight updates, but provide some theoretical guarantees as long as these overwrites are sparse. However, all these prior works are mostly applied to visually simpler domains, or do not fully take advantage of temporally smooth input data, or investigate local communication. Here, we investigate a global, top-down, and yet asynchronous communication between the layers of a neural network during its training. The view that is consistent with many mathematical models of cortex [5, 26, 28, 48]. Finally, most of the works above can also potentially be used together with our *Sideways* training, which we leave as a possible future direction.

Large models. Parallelism has grown in importance due to the success of gigantic neural networks with billions of parameters [49], potentially having high-resolution inputs [39], that cannot fit into individual GPUs. Approaches such as GPipe [18] or DDG [19] show that efficient pipelining strategies can be used to decouple the forward and backward passes by buffering activations at different layers, which then enables the parallel execution of different layers of the network. Similarly, multiple modules of the network can be processed simultaneously on activations belonging to different mini-batches [19]. Such pipelining reduces the training time for image models but at the cost of increased memory footprint.

Efficient video processing. Conditional computation [3] or hard-attention approaches can increase efficiency [32, 34] when dealing with large data streams. These are, however, generic approaches that do not exploit the temporal smoothness of sequential data such as video clips [50]. For video, sampling key frames is shown to be a quite powerful mechanism when performing classification [25, 51], but may not be appropriate if a more detailed temporal representation of the input sequence is needed [13]. Recently, a deep decoupled video model [8] has been proposed that achieves high throughput and speed at inference time, while preserving the accuracy of sequential models. In this paper, we also experiment with parallelizing inference, but go further and make both inference and learning depth-parallel.

3. Sideways

In this section, we define the formulation of our problem and formalize both algorithms: *BP* and *Sideways*.

3.1. Notation and Definitions

We consider the following general setting:

- a finite input time-series $\boldsymbol{x} = (\boldsymbol{x}^t)_{t=1}^K, \boldsymbol{x}^t \in \mathbb{R}^d$, e.g., a video clip with d = height × width × 3,
- a finite output time-series $\boldsymbol{y} = (\boldsymbol{y}^t)_{t=1}^K, \boldsymbol{y}^t \in \mathbb{R}^{d_y}$, e.g., an action label; in the action recognition task, in our work, we use the same label over the whole video clip, i.e., $\boldsymbol{y}^t = \boldsymbol{y}^{t+1}$ for all t,
- a frame-based neural network $\mathcal{M}_\theta : \mathbb{R}^d \to \mathbb{R}^{d_y}$ that transforms the input signal $\boldsymbol{x}^t$ into logits $\boldsymbol{h}_D^t = \mathcal{M}_\theta(\boldsymbol{x}^t)$, and is defined by a composition of modules

  $$\mathcal{M}_\theta(\boldsymbol{x}^t) = H_D(\cdot, \theta_D) \circ H_{D-1}(\cdot, \theta_{D-1}) \circ \ldots \circ H_1(\boldsymbol{x}^t, \theta_1)$$

  where:
  - each module, or layer, $H_i(\cdot,\cdot)$ is a function $H_i : \mathbb{R}^{d_{i-1}} \times \mathbb{R}^{p_i} \to \mathbb{R}^{d_i}$, $i = 1, \ldots D$,
  - $\theta_i \in \mathbb{R}^{p_i}$, $i = 1, \ldots, D$ are the (trainable) parameters, and we use θ for all the parameters,
  - $\circ$ is a composition, i.e., $G \circ F(\boldsymbol{x}) = G(F(\boldsymbol{x}))$

  and
- a loss function $\mathcal{L} : \mathbb{R}^{d_y} \times \mathbb{R}^{d_y} \to \mathbb{R}$, e.g., $\mathcal{L}(\boldsymbol{h}, \boldsymbol{y}) = ||\boldsymbol{h} - \boldsymbol{y}||^2$, or $\mathcal{L}(\boldsymbol{h}, \boldsymbol{y}) = -\sum_i p((\boldsymbol{h})_i) \log q(\boldsymbol{y}_i)$.

We extend the notation above to $\boldsymbol{h}_i^t = H_i(\cdot, \theta_i) \circ H_{i-1}(\cdot, \theta_{i-1}) \circ \ldots \circ H_1(\boldsymbol{x}^t, \theta_1)$.

To avoid the common confusion coming from using the same letters to denote both the function formal arguments and actual values of the variables, we will use bold font for the latter, e.g., x to denote a formal argument and $\boldsymbol{x}$ for its actual value. We also use the following notation for the derivatives of the functions H_i. Let $\mathcal{J}_h H(\boldsymbol{h}, \boldsymbol{\theta}) = \left.\frac{\partial H(h, \boldsymbol{\theta})}{\partial h}\right|_{h=\boldsymbol{h}}$ be the Jacobian matrix of $H(h, \theta)$ with respect to the variable h evaluated at $h = \boldsymbol{h}$, $\theta = \boldsymbol{\theta}$. Similarly, $\mathcal{J}_\theta H(\boldsymbol{h}, \boldsymbol{\theta}) = \left.\frac{\partial H(\boldsymbol{h}, \theta)}{\partial \theta}\right|_{\theta=\boldsymbol{\theta}}$ denote the Jacobian matrix of $H(h, \theta)$ with respect to the variable θ evaluated at $h = \boldsymbol{h}$, $\theta = \boldsymbol{\theta}$. We will use the same notation for the gradient ∇.

Finally, to train neural networks, we base our computations on the empirical risk minimization framework, i.e. $\mathcal{R}(\mathcal{M}_\theta) = E_{x,y}[\mathcal{L}(\mathcal{M}_\theta(x), y)] \approx \sum_{\boldsymbol{x},\boldsymbol{y}\sim\mathcal{D}} \frac{1}{K} \sum_{t=1}^K \mathcal{L}(\boldsymbol{h}_D^t, \boldsymbol{y}^t)$, where $\mathcal{D}$ is a training set.

3.2. Update Cycle

For simplicity, we assume in our modelling a constant time for a layer (or some set of layers organized into a module) to fully process its inputs, both in the forward or backward pass and call this a *computation step*. We define the *update cycle* as the sequence of computation steps that a given data frame is used to update all the layers, and the *cycle length* as the number of computation steps in the update cycle. Hence, the cycle length depends only on the depth of the network D and is equal to $2D - 1$ computation steps. Figure 2 illustrates a single update cycle with nine computation steps for both models.

3.3. The *BP* algorithm ('regular' backpropagation)

The *BP* algorithm refers to regular training of neural networks. Here, due to the synchronization between the passes, computations are blocked each time a data frame is processed. This is illustrated in Figure 2 (left). Whenever the first frame is processed, here indicated by the blue square, the computations are blocked in both forward and backward passes over the whole update cycle.

With our notation, the standard backpropagation formula becomes

$$\begin{aligned}\nabla_{\theta_i}^t \mathcal{L} \;=\; & \nabla_{\theta_i} \mathcal{L}(\mathcal{M}_\theta(\boldsymbol{x}^t), \boldsymbol{y}^t)|_{\theta=\boldsymbol{\theta}} = \\ & \nabla_{h_D} \mathcal{L}(\boldsymbol{h}_D^t, \boldsymbol{y}^t) \cdot \mathcal{J}_{h_{D-1}} H_D(\boldsymbol{h}_{D-1}^t, \boldsymbol{\theta}_D) \cdot \\ & \mathcal{J}_{h_{D-2}} H_{D-1}(\boldsymbol{h}_{D-2}^t, \boldsymbol{\theta}_{D-1}) \cdot \\ & \vdots \\ & \mathcal{J}_{h_i} H_{i+1}(\boldsymbol{h}_i^t, \boldsymbol{\theta}_{i+1}) \cdot \\ & \mathcal{J}_{\theta_i} H_i(\boldsymbol{h}_{i-1}^t, \boldsymbol{\theta}_i)\end{aligned}$$

with the update rule $\theta_i := \theta_i - \alpha \frac{1}{K} \sum_{t=1}^K \nabla_{\theta_i}^t \mathcal{L}$, where α is the learning rate, and K is the length of the input sequence.

We can compactly describe the algorithm above with the following recursive rules

$$\nabla_{\theta_i}^t \mathcal{L} = \nabla_{h_i}^t \mathcal{L} \cdot \mathcal{J}_{\theta_i} H_i(\boldsymbol{h}_{i-1}^t, \boldsymbol{\theta}_i) \quad (1)$$

$$\nabla_{h_{i-1}}^t \mathcal{L} = \nabla_{h_i}^t \mathcal{L} \cdot \mathcal{J}_{h_{i-1}} H_i(\boldsymbol{h}_{i-1}^t, \boldsymbol{\theta}_i) \quad (2)$$

where $\boldsymbol{h}_0^t = \boldsymbol{x}^t$. However, note that in standard implementations, Jacobian matrices are not computed explicitly; instead efficient vector matrix multiplications are used to backpropagate errors from the loss layer towards the input [1].

3.4. *Sideways* algorithm

We aim at pipelining computations for the whole update cycle during training and inference. *Sideways* removes synchronization by continuously processing information, either in the forward or backward pass. This is

illustrated in Figure 2 (right). Once a data frame is available, it is immediately processed and sent to the next layer, 'freeing' the current layer so it can process the next data frame. Hence, in the first computation step of the update cycle, a data frame $\boldsymbol{x}^t$ is processed by the first *Sideways* module, freeing resources and 'sending' $\boldsymbol{h}_1^t$ to the second *Sideways* module at computation step $t+1$. At computation step $t+1$, the first module can now take the next data frame $\boldsymbol{x}^{t+1}$ for processing, and, simultaneously, the second module processes $\boldsymbol{h}_1^t$; this step results in two representations $\boldsymbol{h}_2^t$ and $\boldsymbol{h}_1^{t+1}$. Please note that our notation $\boldsymbol{h}_2^t$ does not indicate the current computation step but instead that the representation has originated at $\boldsymbol{x}^t$. We continue the same process further during the training. This is illustrated in Figure 2, where we use color-encoding to track where the information being processed has originated from. Dotted arrows represents the forward pass.

For simplicity, we assume that the computation of the loss takes no time and does not require an extra computation cycle. In such setting the activation arriving at the loss function computing module at timestep t is $\boldsymbol{h}_D^{t-D+1}$, an activation spawned by the frame $\boldsymbol{x}^{t-D+1}$. Once this final representation $\boldsymbol{h}_D^{t-D+1}$ is computed at computation step t, we calculate its 'correct' gradient $\nabla_{h_D}^t \mathcal{L}(\boldsymbol{h}_D^{t-D+1}, \boldsymbol{y}^t)$, and we backpropagate this information down towards the lower layers of the neural network. This computational process is illustrated in Figure 2 (right) by the solid arrows.

Let us formalize this algorithm in a similar manner to the 'regular' backpropagation. In the *Sideways* algorithm the gradient $\nabla_{\theta_i}\mathcal{L}|_{(\boldsymbol{x}^t,\boldsymbol{\theta}_i)}$ is replaced with a *pseudo-gradient* $\widetilde{\nabla}_{\theta_i}\mathcal{L}|_{(\boldsymbol{x}^t,\boldsymbol{\theta}_i)}$, defined as follows

$$\begin{aligned}\widetilde{\nabla}_{\theta_i}^t\mathcal{L} \;=\; & \nabla_{h_D}\mathcal{L}(\boldsymbol{h}_D^{t_i-D+1}, \boldsymbol{y}^{t_i}) \cdot \mathcal{J}_{h_{D-1}} H_D(\boldsymbol{h}_{D-1}^{t_i-D+1}, \boldsymbol{\theta}_D) \cdot \\ & \mathcal{J}_{h_{D-2}} H_{D-1}(\boldsymbol{h}_{D-2}^{t_i-D+3}, \boldsymbol{\theta}_{D-1}) \cdot \\ & \vdots \\ & \mathcal{J}_{h_i} H_{i+1}(\boldsymbol{h}_i^{t-i-1}, \boldsymbol{\theta}_{i+1}) \cdot \\ & \mathcal{J}_{\theta_i} H_i(\boldsymbol{h}_{i-1}^{t-i+1}, \boldsymbol{\theta}_i)\end{aligned}$$

where $t_i = t + i - D$.

The equations above can next be written succinctly and recursively as the *Sideways* backpropagation rules

$$\widetilde{\nabla}_{\theta_i}^t\mathcal{L} \;=\; \widetilde{\nabla}_{h_i}^{t-1}\mathcal{L} \cdot \mathcal{J}_{\theta_i} H_i(\boldsymbol{h}_{i-1}^{t-i+1}, \boldsymbol{\theta}_i) \qquad (3)$$

$$\widetilde{\nabla}_{h_{i-1}}^t\mathcal{L} \;=\; \widetilde{\nabla}_{h_i}^{t-1}\mathcal{L} \cdot \mathcal{J}_{h_{i-1}} H_i(\boldsymbol{h}_{i-1}^{t-i+1}, \boldsymbol{\theta}_i) \qquad (4)$$

where $\widetilde{\nabla}_{h_D}^{t-1}\mathcal{L} = \nabla_{h_D}\mathcal{L}(\boldsymbol{h}_D^{t-D+1}, \boldsymbol{y}^t)$, and $\boldsymbol{h}_0^t = \boldsymbol{x}^t$.

In the equations above, we use a color-encoding similar to Figure 2 (right) to indicate that we combine information originated from different time steps. For instance, information originated in 'blue' and 'yellow' input frames is combined (6-th computation step and second-last unit) as indicated by the red circle in Figure 2 (right)). By following the arrows we can track the origins of the combined information.

Due to the nature of these computations, we do not compute proper gradients as the *BP* algorithm does, but instead we compute their more noisy versions, $\widetilde{\nabla}_{\boldsymbol{h}_i}\mathcal{L} = \nabla_{\boldsymbol{h}_i}\mathcal{L} + \epsilon_i(\boldsymbol{x})$, which we call pseudo-gradients. The amount of noise varies with respect to the smoothness of the input $\boldsymbol{x}$, and the number of the layer i. That is, deeper layers have less noisy pseudo-gradients, and e.g., the pseudo-gradient of the final layer is exact.

We organize training as a sequence of episodes. Each episode consists of one or more update cycles, runs over the whole sampled video clip $\boldsymbol{x}$ or its subsequence, and ends with the weights update. We assume the input $\boldsymbol{x}$ is smooth within the episode, e.g., $\boldsymbol{x}$ is a video of an action being performed with a reasonable frame-rate. We 'restart' *Sideways* by setting up all the activations and pseudo-gradients to zero whenever we sample a new video to avoid aliasing with a pseudo-gradient originated from a data frame from another video clip, and thus breaking our assumptions about the smoothness of the input sequence. Mini-batching can optionally be applied in the usual way.

We average gradients computed at each layer over all computation steps within the episode, i.e.,

$$\widetilde{\nabla}_{\theta_i}\mathcal{L} = \frac{1}{L}\sum_{t=1}^{L}\widetilde{\nabla}_{\theta_i}^t\mathcal{L} \qquad (5)$$

where L is the length of the episode. In our experiments we consider two cases. In the *classification* task, the episode is the same as the sampled sequence, i.e., $L = K$. In the *auto-encoding* task, the episode is a single data frame, i.e., $L = 1$. We use pseudo-gradients $\widetilde{\nabla}_{\theta_i}\mathcal{L}$ for the weight updates, i.e., $\theta_i := \theta_i - \alpha\widetilde{\nabla}_{\theta_i}\mathcal{L}$.

Figure 3 (right) illustrates the situation when the pipeline is full and suggests, the information flow is tilted sideways. Therefore, there is no information available in the upper layers at the beginning of the sequence (empty circles in the figure). For that reason, we modify Equation 5 by including a binary mask, i.e., $\widetilde{\nabla}_{\theta_i}\mathcal{L} = \frac{1}{\gamma_i}\sum_{t=1}^{L}\gamma_i^t\widetilde{\nabla}_{\theta_i}^t\mathcal{L}$, where $\gamma_i = \sum_t \gamma_i^t$. The mask is zero for unavailable gradients. For similar reasons, to avoid gradient computations whenever suitable information is unavailable, we modify Equation 4 with $\widetilde{\nabla}_{\boldsymbol{h}_i}^t\mathcal{L} = \gamma_i^t\widetilde{\nabla}_{h_i}^{t-1}\mathcal{L} \cdot \mathcal{J}_{h_{i-1}} H_i(\boldsymbol{h}_{i-1}^{t-i+1}, \boldsymbol{\theta}_i)$. Without masking, we have observed more unstable training in practice.

Intuitions. As we make the input sequence increasingly

more smooth, in the limits, each data frame has identical content. In such a case, since $\epsilon_i(\boldsymbol{x}) = 0$, pseudo-gradients equal gradients, and our algorithm is the same as the 'regular' backpropagation. In practice, if the input sequence has different data frames, we assume that two consecutive frames are similar, and especially essential features are slowly evolving, sharing their semantics within the neighborhood [50].

4. Experiments

We investigate both algorithms – *BP* and *Sideways* – on several benchmarks. Since, to the best of our knowledge, this is possibly the first work on depth-parallel training on challenging video tasks, we focus on simple convolutional networks, and aim to explore the training dynamics instead of seeking state-of-the-art results. We leave data augmentation, additional features such as optical flow, or pre-training on large datasets [7, 11, 22, 23, 43] for future work. We compare frame-based video models [22, 23, 43] trained either using *BP* or *Sideways* that are *trained from scratch* and using standard setups.

4.1. Task

We benchmark our algorithms on two different tasks and three datasets.

Classification. We start with the classical classification task, here, in the form of action recognition. Since the classification is at the core of regular supervised learning, we believe, any alternative, sequential or parallel, to SGD should be evaluated on this common task. Figure 2 illustrates both algorithms under the classification scenario. Differently to the next, auto-encoding task, here, we test the networks under the regular circumstances, where each frame is always guaranteed to be processed by the neural network.

Auto-encoding. While majority of our key results are on the classification task, it is also informative to validate *Sideways* on tasks where the target output is continuously changing with the input. As a proof of concept, we experiment here with the simpler task of auto-encoding. To clearly illustrate advantages of *Sideways* training, and for the sake of simplicity, we assume that the input frame rate and the processing time for each individual neural network layer are equal. This is shown in Figure 3. If the stream is a sequence $(x^{t_1}, x^{t_2}, x^{t_3}, \ldots)$, D is the number of modules, then *BP* blocks the processing of the input for $2(D-1)$ computation steps, hence ignoring data frames between t_1 and t_{10} during training for $D = 5$. This is illustrated in Figure 3 (left). In contrast, *Sideways* pipelines computations and uses all the data frames in both training and inference modes. This often results in superior performance of *Sideways* under the circumstances mentioned above. Finally, by comparing Figures 2 and 3, we can clearly see the *Sideways* algorithm behaves identically, even if we artificially introduce the blocking mechanism described above.

4.2. Datasets

We choose to benchmark our models of computations on the following video datasets. On one hand, first two datasets have enough complexity and realism. On the other hand, we can easily train frame-based video models on all the following datasets.

HMDB51 is a widely used dataset for action recognition that has 6770 video clips representing 51 actions [27]. Video clips run at 30fps. In our experiments, we use the first train and test splits, similar to ablation studies in [22, 43]. This is the smallest real-world dataset in our experiments, and since training is fast, we therefore use mainly this setting to study our models in details.

UCF101 is another popular dataset for action recognition [45]. It has 13320 videos clips and 101 human actions. Actions include pizza tossing, typing, playing cello, skiing, etc. Default frame-rate is 25fps, with the duration of 7.21sec on average. Each frame has resolution 320-by-240. We use train and test splits in our studies. In our experiments, we find this dataset to be of particular interest due to its size, complexity, and realism.

CATER dataset [13] provides synthetically generated videos of moving simple 3D objects. We use only the video frames and we set up an unsupervised auto-encoding task. These videos have two desired properties – i) they are visually simple, and ii) they have diverse motion patterns of various objects – making it an excellent benchmark for *Sideways*. We use the pre-generated video sequences provided by the authors in the *all_actions* subset, consisting of 3861 training video sequences and 1639 test sequences, each with 300 frames, having 320-by-240 pixels resolution at 24fps.

4.3. Architectures

For the purposes of our study we have experimented with two standard convolutional network architectures. The first one is organized into 6 *Sideways* modules, another one with 8 *Sideways* modules. Note, however, that we can use more than one trainable layers inside a single *Sideways* module.

Simple-CNN is a simple and fast baseline consisting of 5 convolutional layers with kernel size $3x3$ followed by global average pooling and a softmax on the linear layer that projects the internal representation into classes. The convolutional layers have the following number of channels: $(32, 64, 64, 128, 256)$. To reduce resolution

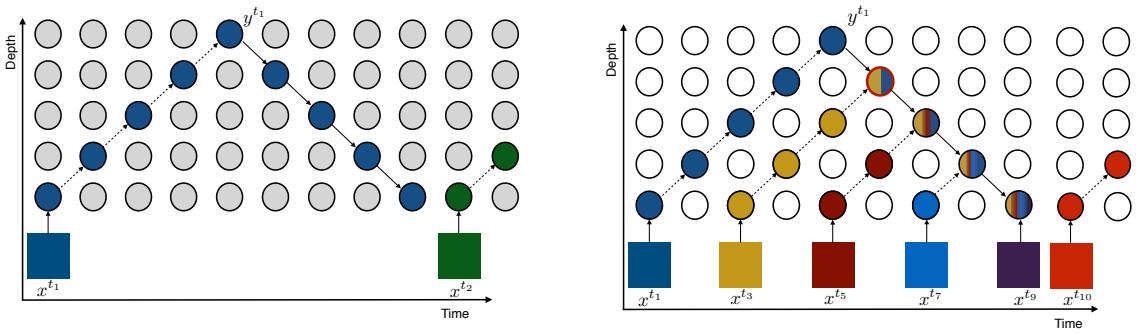


Figure 2 | From left to right. Standard (*BP*) and fully pipelined (*Sideways*) approaches to temporal training and inference. We show a single update cycle, and the beginning of the next cycle. Both architectures are unrolled in time. Colorful squares indicate data frames. Circles indicate 'regular' or *Sideways* modules. Dotted arrows show how information is passed between layers and time steps in forward pass. Solid arrows show the same in backward pass. In *Sideways* (right), we only exemplify a single update path with the arrows, and use empty circles for all other units. Gray circles denote blocked modules, i.e., units waiting for forward or backward pass. Note that for *BP*, we use the same color for all the units on the data path, in both the forward and the backward passes, to highlight that all the layers work on information originated in a single data frame, the blue one. Differently, the back-pass in *Sideways* shows circles with many colors to illustrate that information from different data frames is combined in one update cycle. For instance, combining 'blue gradient' with 'yellow activations' yields 'blue-yellow gradient' (6th computation step and second-last unit). Best viewed in color.

progressively in the network, we use striding 2 in every second layer starting from the first one.

For the auto-encoding experiments, we train a simple encoder-decoder architecture having the same five convolutional blocks followed by symmetrical five deconvolutional blocks. We use *Sideways* blocks only for the convolutional encoder; the decoder layers are connected all in a single sequential block, and hence the decoder-block is trained with a regular *BP* with 'correct' gradients. For simplicity, we also assume the whole decoder takes just a single computation step. We use this setting to better investigate the quality of the features extracted by the *Sideways* encoder.

VGG-net refers to VGG-8, which is a direct re-implementation of the RGB network in the original two-stream model [44] with the addition of batchnorm in every VGG-block (in between the convolution and the ReLU).

Implementation details. By default, we use gradient clipping by value 1.0. We use a bias term only on the last linear layer used to produce logits. We considered three different popular optimizers: SGD, SGD with momentum, and Adam [24]. We use default hyperparameters for all of them and our observation is that *Sideways* is stable under all the considered training algorithms so we report results with Adam only. We use a warm-up scheme by linearly interpolating learning rate in each iteration between 0 at the beginning and the initial value at the 5-th epoch. Later we drop the learning rate by dividing it by 10 at 100-th and 200-th epochs. We use Tensorflow 2 [1] to implement our framework.

In some experiments we use batchnorm [20] and dropout [46] in linear layers (0.9 as [43]). In most training experiments, we use a single GPU (V100) – but measure parallelization speedup later in the section using multiple GPUs. We decouple the weight decay term from the loss [30] and find that some amount of weight decay is beneficial for generalization of the VGG-net models. We do a hyper-parameter search over the weight decay coefficient (possible values are: $0.0, 10^{-4}, 10^{-3}, 10^{-2}$), and over the initial learning rate (either 10^{-4} or 10^{-5}), fairly for both types of training.

We train on videos with the per-frame resolution 112-by-112 and a sequence length 64 randomly cropped from the whole video clip as a contiguous subsequence. We also use random flipping during training, and this augmentation is performed consistently over all the frames in every clip. At test time we simply take a center crop of a video frame. In all cases, we use torus-padding (video frames are repeated) whenever a sampled video clip is shorter than 64 and at test time we evaluate over the whole video sequence. In practice we use a fixed batch size of 8 videos for training.

For the auto-encoding experiments with CATER, we use square crops of 240×240 pixels, extracted randomly during training and central crops of the same size during testing.

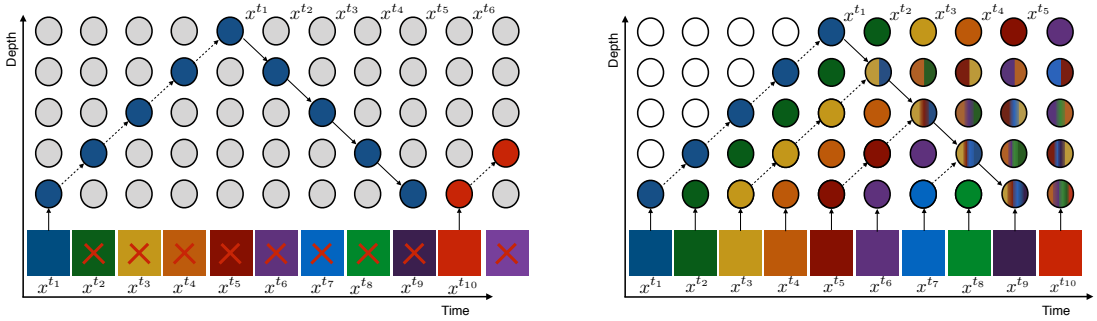


Figure 3 | From left to right. *BP* and *Sideways* approaches to temporal training and inference. In the figure, we illustrate the auto-encoding task, where the network needs to synthesize input frames. Crossed frames denote input data ignored because the system cannot operate in real-time to process all the inputs (left). In contrast, *Sideways* works simultaneously at full capacity once the pipeline is full; and since we show the beginning of the episode some units are unused (empty circles) due to the shape of the data flow (right). All the colors and arrows have the same meaning as in Figure 2. Best viewed in color.

HMDB51	*BP*	*Sideways*
Simple-CNN	17.2	16.5
VGG-8	24.6	25.8
3DResNet (scratch) [15, 22]	17.0	-
UCF101	***BP***	***Sideways***
Simple-CNN	40.7	42.16
VGG-8	49.1	53.8
VGG-8 + Dropout (0.9)	56.0	58.2
VGG-8 (scratch)+ Dropout (0.9) [43]	52.3	-
3DResNet (scratch) [15, 22]	42.5	-

Table 1 | Comparison of our implementation of two architectures using *Sideways* and *BP* computational models on different datasets. For reference, we also report similar models from prior work [15, 22, 43]. We report accuracy in %.

4.4. Results (Classification)

We have evaluated networks trained with *Sideways* and *BP* according to the regular accuracy metric. Moreover, to gain a better understanding, and to show how general the *Sideways* training is, we have conducted several different experiments measuring not only accuracy but also training dynamics and robustness of the method.

Quantitative results. Table 1 directly compares both algorithms, backpropagation with the pipelined *Sideways* training. For the sake of comparison, we also report referenced models that are trained using 'regular' training. As we can see, we have reproduced similar results with the *BP* model, and in several cases, we have achieved higher accuracy (e.g., VGG-8 + Dropout (0.9)). Even though higher accuracy numbers have been previously reported on both datasets, these are achieved using larger models pre-trained on larger datasets. Our focus is, however, different.

Results presented in Table 1 suggest that the *Sideways* training achieves competitive accuracy to *BP*, and the introduced noise due to i) the sampling error, the same as SGD updates, and ii) the pseudo-gradients computations, does not seem to harm the overall performance. Quite the opposite, under certain conditions, we observe *Sideways* generalizes better than *BP*. Since such behavior occurs during training larger models on relatively small video datasets, e.g., training VGG-8 on UCF-101, which often results in overfitting [43], we hypothesize *Sideways* acts as an implicit regularizer for video processing [35, 52].

Training dynamics. Since we compare *Sideways* algorithm to *BP*, it is instructive to investigate their training behavior. Intuitively, similar training behavior should result in a similar final performance. Therefore, we have conducted experiments where we measure various statistics throughout training, and we report them in Figure 4. There are a few interesting observations. First, the training dynamics of the VGG-8 architecture with *Sideways* training closely follows 'regular' training (first two columns). However, for the Simple-CNN architecture, training dynamics between both algorithms differ under some choice of the hyper-parameters. For instance, we can notice in Figure 4 (last two columns) the loss function become quite unstable. This happens consistently with a larger learning rate, e.g., above 10^{-4}. though this seemingly should also transfer into unstable training accuracy, we have found training does not collapse. Quite the opposite, we report a relatively high training accuracy (above 85%) as shown in Figure 5. After a more careful inspection, we observe that Simple-

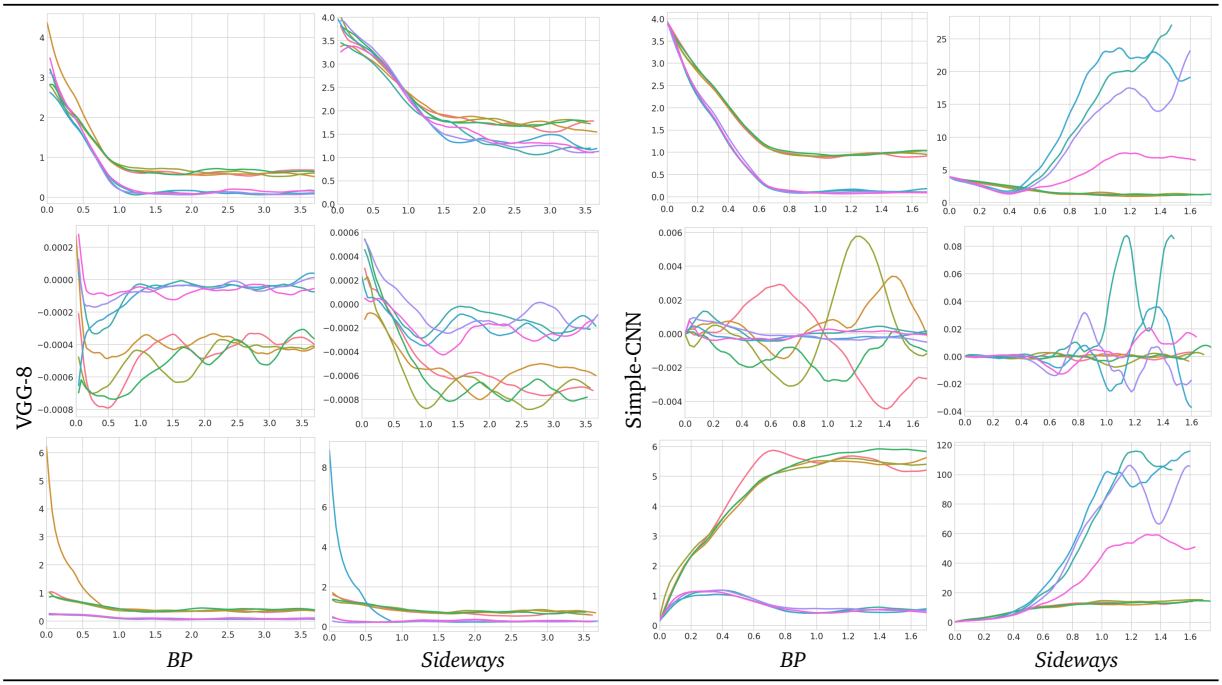


Figure 4 | Training dynamics of Simple-CNN and VGG-8 with different models of computations. Experiments are conducted on the HMDB51 dataset. Different colors denote different hyper-parameters (red, green, olive, orange refer to the initial learning rate 10^{-5} and teal, pink, violet, blue to 10^{-4}, all with various weight decay). On the x-axis, we report number of iteration steps, in 10^5 scale. On the y-axis, we report, from the top to bottom: loss, mean of the gradients, and average gradient magnitude (l2-norm). Note that the figures have different y-limits to allow a detailed visualization of the training dynamics as training progresses.

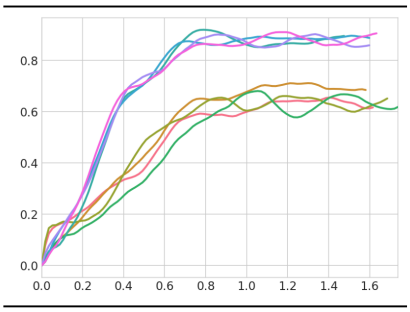


Figure 5 | Training of Simple-CNN with the *Sideways* algorithm on HMDB51. Different colors denote different hyper-parameters (the same as Figure 4). On the x-axis, we report number of iteration steps, in 10^5 scale. On the y-axis, we report, accuracy numbers.

CNN trained with *Sideways* and larger learning rates tends to give confident predictions that result in high loss whenever they miss the class. Results on UCF-101 are similar, but slightly less pronounced.

Sensitivity to frame rate. The smoothness of the input space is the key underlying assumption behind the *Sideways* algorithm. When the input space is the space of video clips, this assumption translates, e.g., into a high frame-rate. To further stretch this assumption, we have artificially decreased the frame-rate by skipping data frames in the input video clip. This can easily be implemented with the striding operation, i.e., we skip k frames with striding $k+1$. To keep the length of video clips unchanged between the experiments, we sample $k+1$ times longer input sequences, with padding, before we apply striding. We have experimented with striding in $\{2, 3, 4, 5, 6\}$. In our experiments, we have found *Sideways* to be surprisingly robust to the changes in striding. Only some choice of the hyper-parameters, e.g., relatively high learning rate, have resulted in the performance collapse, where the network has transitioned from high into low training accuracies. Nonetheless, *BP* and *Sideways* never collapses with the same set of the carefully chosen hyper-parameters. Distortions introduced by padding could be another explanation for the collapse of models trained with 'unfavorable' hyper-parameters and higher striding numbers. We report these results in Figure 6.

Training speed-up using multiple GPUs. We evaluate the speedup obtained when training the VGG-8 and Simple-net models using a single V100 GPU per module – 8 for VGG and 6 for Simple-net. To isolate training

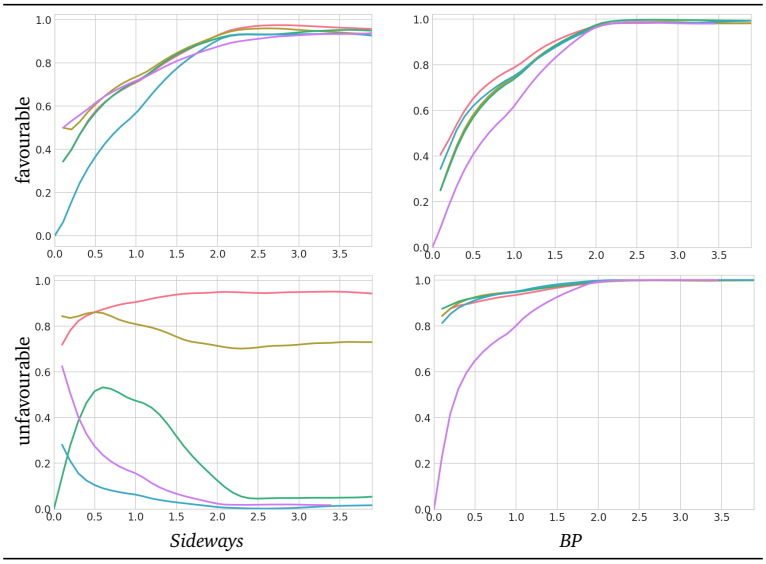


Figure 6 | We experiment with different temporal striding settings ($\{2, 3, 4, 5, 6\}$ encoded as red, olive, green, blue, violet, respectively) for the input videos, on UCF101. Top row shows favourable hyper-parameters (initial learning rate equals to 10^{-5}). Bottom row shows unfavourable hyper-parameters (initial learning rate equals to 10^{-4}). First column shows *Sideways*. Second column shows *BP*. On the x-axis, we report number of iteration steps. On the y-axis, we report accuracy numbers. In the setting with unfavourable hyper-parameters, training of networks with higher striding numbers collapse.

	BP	*Sideways*	speedup
Simple CNN	1.7	8.4	4.9x
VGG-8	0.1	0.6	6.0x

Table 2 | Number of training steps per second for two architectures, using batch size of 8 clips, each having 64 frames and resolution 112x112. The results were obtained using one GPU per network module (6 for Simple CNN and 8 for VGG-8).

speed from the data loading aspect, in this study, we artificially construct videos consisting of random numbers. We train each model for 100 steps, repeat this 3 times and return the highest average number of training steps per second. The results are shown in Table 2, which validate that there is a large speed-up for *Sideways* when parallel resources are assigned along the network depth. In particular, VGG has a more balanced decomposition in terms of FLOPs per module. The *BP* model benefits little from the multiple GPUs since they are locked most of the time waiting for the other GPUs to complete their processing. Note also, that placing different *Sideways* modules in different GPUs will also significantly reduce memory requirements for training large neural networks.

4.5. Results (Auto-Encoding)

We evaluate both algorithms using mean squared error, between pixels, between the predicted and the ground truth sequences, under the same conditions, in particular, under the same frame rate.

Qualitative results. We show qualitative results of the *BP* outputs in Figure 7 and *Sideways* outputs in Figure 8. Shapes, colors, as well as many fine-grained attributes such as metallic materials are properly decoded. We have found that the model trained with *BP* is successful at decoding coarser objects attributes, but is slightly less accurate with metallic materials. As mentioned above, because of the blocking mechanism of the *BP* algorithm and the high frame rate of the input, the method needs to discard input frames to not accumulate latency. In these cases, the last produced output is copied to compensate for the low output rate, resulting in identical output frames at different time steps over some time interval – and different ones at the beginning of the next update cycle (this is best visible in the 1st row of Figure 7).

Quantitative results. Table 3 shows mean squared error (the lower, the better) between predicted frames and ground truth (input frames). We compare the same architecture trained with *Sideways* and the regular *BP*. Because of the synchronization, the method trained with *BP* cannot output at a fast enough pace to keep up with the input frame rate, which yields a significant error.

	BP	*Sideways*
Auto-encoding	0.014	0.002

Table 3 | Mean squared error between predictions and ground truth data; the lower, the better.

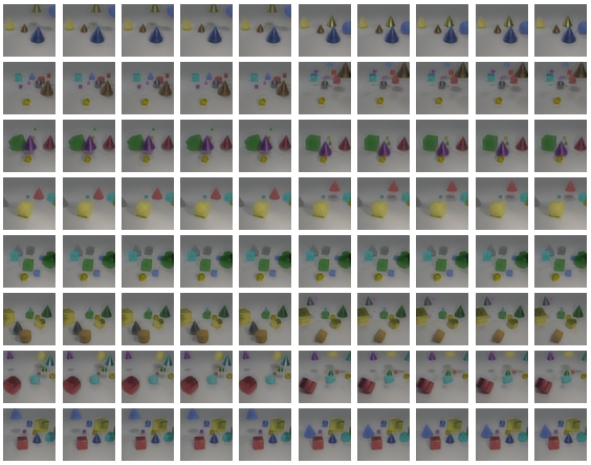


Figure 7 | Auto-encoding results for *BP*. Each row shows an individual video sequence consisting of, in our case, 64 frames. For the sake of visualization, we sub-sample 10 consecutive middle frames from the outcome.



Figure 8 | Auto-encoding results for *Sideways*. Each row shows an individual video sequence consisting of, in our case, 64 frames. For the sake of visualization, we sub-sample 10 consecutive middle frames from the outcome.

These results show that the proposed training scheme can be successfully applied also to tasks where both input and output are continuously evolving, reducing considerably the latency of the system during training. Together with the results on the classification task, we conclude that this training scheme is general enough to be applied for a wide range of video tasks.

5. Conclusion

We have proposed *Sideways* – a backpropagation variant to train networks, where activations from different computation steps are used in the weight updates. We motivate our training algorithm by the smoothness of video signals, and especially we assume that important features vary slowly, at least in the latent space [17, 50].

We have found that *Sideways* is not only a valid learning mechanism but can also potentially provide an implicit regularization during the training of neural networks. Decoupling provided by the *Sideways* algorithm makes it especially attractive for training large models in parallel.

We hope that our work will spark further interest in developing decoupled training of more advanced temporal models or in a better understanding of the role of slow features, temporal redundancies, and stochasticity in the learning process of such models. Although biological plausibility is not our primary motivation, we believe our architecture has some desired properties. For instance, top-down and global communication implemented in *Sideways* does not necessarily require neither depth-synchronization nor instantaneous propagation; it also does not require local caching of the activations during the weights updates for the backward pass. Finally, its unrolling in time could be viewed as more biologically correct [5, 26].

References

[1] M. Abadi, A. Agarwal, P. Barham, E. Brevdo, Z. Chen, C. Citro, G. S. Corrado, A. Davis, J. Dean, M. Devin, et al. Tensorflow: Large-scale machine learning on heterogeneous distributed systems. arXiv preprint arXiv:1603.04467, 2016.

[2] D. Balduzzi, H. Vanchinathan, and J. Buhmann. Kickback cuts backprop's red-tape: Biologically plausible credit assignment in neural networks. In AAAI Conference on Artificial Intelligence, 2015.

[3] E. Bengio, P.-L. Bacon, J. Pineau, and D. Precup. Conditional computation in neural networks for faster models. In 2nd Multidisciplinary Conference on Reinforcement Learning and Decision Making (RLDM), 2015.

[4] Y. Bengio, D.-H. Lee, J. Bornschein, T. Mesnard, and Z. Lin. Towards biologically plausible deep learning. arXiv preprint arXiv:1502.04156, 2015.

[5] A. Betti and M. Gori. Backprop diffusion is biologically plausible. arXiv preprint arXiv:1912.04635, 2019.

[6] L. Bottou and Y. L. Cun. Large scale online learning. In Advances in Neural Information Processing Systems (NeurIPS), 2004.

[7] J. Carreira and A. Zisserman. Quo vadis, action recognition? a new model and the kinetics dataset. In Conference on Computer Vision and Pattern Recognition (CVPR), 2017.

[8] J. Carreira, V. Patraucean, L. Mazare, A. Zisserman, and S. Osindero. Massively parallel video networks. In European Conference on Computer Vision (ECCV), 2018.

[9] A. Choromanska, M. Henaff, M. Mathieu, G. B. Arous, and Y. LeCun. The loss surfaces of multilayer networks. In Artificial Intelligence and Statistics, 2015.

[10] W. Czarnecki, G. Świrszcz, M. Jaderberg, S. Osindero, O. Vinyals, and K. Kavukcuoglu. Understanding synthetic gradients and decoupled neural interfaces. In International Conference on Machine Learning (ICML), 2017.

[11] A. Diba, V. Sharma, L. Van Gool, and R. Stiefelhagen. Dynamonet: Dynamic action and motion network. In IEEE International Conference on Computer Vision (ICCV), 2019.

[12] J. Duchi, E. Hazan, and Y. Singer. Adaptive subgradient methods for online learning and stochastic optimization. Journal of Machine Learning Research (JMLR), 2011. ISSN 1532-4435.

[13] R. Girdhar and D. Ramanan. Cater: A diagnostic dataset for compositional actions and temporal reasoning. International Conference on Learning Representations (ICLR), 2020.

[14] P. Goyal, P. Dollár, R. Girshick, P. Noordhuis, L. Wesolowski, A. Kyrola, A. Tulloch, Y. Jia, and K. He. Accurate, large minibatch sgd: Training imagenet in 1 hour. arXiv preprint arXiv:1706.02677, 2017.

[15] K. Hara, H. Kataoka, and Y. Satoh. Can spatiotemporal 3d cnns retrace the history of 2d cnns and imagenet? In Computer Vision and Pattern Recognition (CVPR), 2018.

[16] K. He, R. Girshick, and P. Dollár. Rethinking imagenet pre-training. In International Conference on Computer Vision (ICCV), 2019.

[17] G. E. Hinton. Connectionist learning procedures. In Machine learning, pages 555–610. Elsevier, 1990.

[18] Y. Huang, Y. Cheng, D. Chen, H. Lee, J. Ngiam, Q. V. Le, and Z. Chen. Gpipe: Efficient training of giant neural networks using pipeline parallelism. In Advances in Neural Information Processing Systems (NeurIPS), 2018.

[19] Z. Huo, B. Gu, Q. Yang, and H. Huang. Decoupled parallel backpropagation with convergence guarantee. In International Conference on Machine Learning (ICML), volume 80, 2018.

[20] S. Ioffe and C. Szegedy. Batch normalization: Accelerating deep network training by reducing internal covariate shift. In International Conference on Machine Learning (ICML), 2015.

[21] M. Jaderberg, W. M. Czarnecki, S. Osindero, O. Vinyals, A. Graves, D. Silver, and K. Kavukcuoglu. Decoupled neural interfaces using synthetic gradients. In International Conference on Machine Learning (ICML), 2017.

[22] L. Jing and Y. Tian. Self-supervised spatiotemporal feature learning by video geometric transformations. arXiv preprint arXiv:1811.11387, 2018.

[23] A. Karpathy, G. Toderici, S. Shetty, T. Leung, R. Sukthankar, and L. Fei-Fei. Large-scale video classification with convolutional neural networks. In Computer Vision and Pattern Recognition (CVPR), 2014.

[24] D. Kingma and J. Ba. Adam: A method for stochastic optimization. International Conference on Learning Representations (ICLR), 12 2014.

[25] B. Korbar, D. Tran, and L. Torresani. Scsampler: Sampling salient clips from video for efficient action recognition. In 2011 International Conference on Computer Vision (ICCV), 2019.

[26] J. Kubilius, M. Schrimpf, A. Nayebi, D. Bear, D. L. Yamins, and J. J. DiCarlo. Cornet: modeling the neural mechanisms of core object recognition. BioRxiv, 2018.

[27] H. Kuehne, H. Jhuang, E. Garrote, T. Poggio, and T. Serre. Hmdb: a large video database for human motion recognition. In 2011 International Conference on Computer Vision (ICCV), 2011.

[28] M. Larkum. A cellular mechanism for cortical associations: an organizing principle for the cerebral cortex. Trends in neurosciences, 36(3):141–151, 2013.

[29] T. P. Lillicrap, D. Cownden, D. B. Tweed, and C. J. Akerman. Random synaptic feedback weights support error backpropagation for deep learning. Nature Communications, 2016.

[30] I. Loshchilov and F. Hutter. Decoupled weight decay regularization. In International Conference on Learning Representations (ICLR), 2019.

[31] S. Löwe, P. O'Connor, and B. Veeling. Putting an end to end-to-end: Gradient-isolated learning

of representations. In Advances in Neural Information Processing Systems (NeurIPS), 2019.

[32] M. Malinowski, C. Doersch, A. Santoro, and P. Battaglia. Learning visual question answering by bootstrapping hard attention. In European Conference on Computer Vision (ECCV), 2018.

[33] L. Metz, N. Maheswaranathan, B. Cheung, and J. Sohl-Dickstein. Learning unsupervised learning rules. In International Conference on Learning Representations (ICLR), 2019.

[34] V. Mnih, N. Heess, A. Graves, et al. Recurrent models of visual attention. In Advances in Neural Information Processing Systems (NeurIPS), 2014.

[35] B. Neyshabur. Implicit regularization in deep learning. arXiv preprint arXiv:1709.01953, 2017.

[36] A. Nøkland. Direct feedback alignment provides learning in deep neural networks. In Advances in Neural Information Processing Systems (NeurIPS), 2016.

[37] A. Nøkland and L. H. Eidnes. Training neural networks with local error signals. arXiv preprint arXiv:1901.06656, 2019.

[38] A. v. d. Oord, Y. Li, and O. Vinyals. Representation learning with contrastive predictive coding. arXiv preprint arXiv:1807.03748, 2018.

[39] E. Real, A. Aggarwal, Y. Huang, and Q. V. Le. Regularized evolution for image classifier architecture search. In AAAI Conference on Artificial Intelligence (AAAI), 2019.

[40] B. Recht, C. Re, S. Wright, and F. Niu. Hogwild: A lock-free approach to parallelizing stochastic gradient descent. In Advances in neural information processing systems, 2011.

[41] H. Robbins and S. Monro. A stochastic approximation method. The annals of mathematical statistics, 1951.

[42] Z. Shen, Z. Liu, J. Li, Y.-G. Jiang, Y. Chen, and X. Xue. Object detection from scratch with deep supervision. IEEE Transactions on Pattern Analysis and Machine Intelligence (TPAMI), 2019.

[43] K. Simonyan and A. Zisserman. Two-stream convolutional networks for action recognition in videos. In Advances in Neural Information Processing Systems (NeurIPS), 2014.

[44] K. Simonyan and A. Zisserman. Very deep convolutional networks for large-scale image recognition. International Conference on Learning Representations (ICLR), 2015.

[45] K. Soomro, A. R. Zamir, and M. Shah. Ucf101: A dataset of 101 human actions classes from videos in the wild. arXiv preprint arXiv:1212.0402, 2012.

[46] N. Srivastava, G. Hinton, A. Krizhevsky, I. Sutskever, and R. Salakhutdinov. Dropout: a simple way to prevent neural networks from overfitting. The journal of machine learning research (JMLR), 15(1):1929–1958, 2014.

[47] I. Sutskever, J. Martens, G. Dahl, and G. Hinton. On the importance of initialization and momentum in deep learning. In International Conference on International Conference on Machine Learning (ICML), 2013.

[48] H. Tomita, M. Ohbayashi, K. Nakahara, I. Hasegawa, and Y. Miyashita. Top-down signal from prefrontal cortex in executive control of memory retrieval. Nature, 401(6754), 1999.

[49] A. Vaswani, N. Shazeer, N. Parmar, J. Uszkoreit, L. Jones, A. N. Gomez, Ł. Kaiser, and I. Polosukhin. Attention is all you need. In Advances in Neural Information Processing Systems (NeurIPS), 2017.

[50] L. Wiskott and T. J. Sejnowski. Slow feature analysis: Unsupervised learning of invariances. Neural computation, 14(4):715–770, 2002.

[51] W. Wu, D. He, X. Tan, S. Chen, and S. Wen. Multi-agent reinforcement learning based frame sampling for effective untrimmed video recognition. CoRR, abs/1907.13369, 2019.

[52] C. Zhang, S. Bengio, M. Hardt, B. Recht, and O. Vinyals. Understanding deep learning requires rethinking generalization. International Conference on Learning Representations (ICLR), 2017.

[53] T. Zhang. Solving large scale linear prediction problems using stochastic gradient descent algorithms. In International Conference on Machine learning (ICML). ACM, 2004.

Acknowledgements

We thank Jean-Baptiste Alayrac, Carl Doersch, Tamara Norman, Simon Osindero, and Andrew Zisserman for their critical feedback, and their help during the duration of this project.